RESEARCH PAPER

Nano Science and Technology Journal 1(1) 31-37 Summer 2023

Effect of different thickness Ni layers on morphology and structural properties of Cu-Ni thin films

Vali Dalouji*[1], Samira Goudarzi[1]

[1]*Department of Physics, Faculty of Science, Malayer University, Malayer, Iran*

Article History:
Received 07 August 2023
Accepted 20 September 2023
Published 22 September 2023

Keywords:
Ni layer thicknesses
Morphology
Bearing Area
Absorption coefficient

*Corresponding Authors Email:
dalouji@yahoo.com

DOI: 10.22034/nstj.2023.707955

Abstract

The purpose of this article is to fabricate Cu-Ni nanoparticles of different sizes to investigate the morphology and structural properties of these nanoparticles. Cu-Ni nanoparticles with different nickel layer thicknesses were deposited with capacitive capacitance using a radio frequency plasma enhanced chemical vapor deposition (RF-PECVD) system. The 15 nm thick Ni films have a phase shift of about 25 nm compared to the other films, indicating that the films are firstly very smooth and secondly capable of phase change. Cu NPs without Ni, Cu NPs with 5 nm of Ni and 10 nm of Ni have cavity coverage of less than 5% and layer content of about 90% and 95% which are monolayer heights. Increasing the thickness of nickel affects the index of absorption coefficient of Cu-Ni thin films.

1. Introduction

Recently, nanomaterials as reported by several researchers, have found wide application in several fields of technology [1-4]. Copper-nickel nanoparticles (Cu-Ni NPs) have attracted attention for their potential applications in magneto-optical recording, spintronic devices and data storage, interconnects, and giant magnetoresistance (GMR) [5]. Copper-nickel nanoparticles for the synthesis of dimethyl carbonate and carbon nanotubes have been used as catalysts [6-8]. Carbon nanotubes (CNTs) have received a lot of attention due to their exceptional optical, electrical, and mechanical properties and their attractive potential applications [9-11]. Plasma arc evaporation is used to make copper-nickel nanoparticles [12]. Copper-nickel nanoparticles were grown by electrode position [5]. Copper-nickel nanoparticles are also made by sol-gel method [13]. Among the various methods, the CVD technique has attracted much attention because it provides a way for directional growth [10, 14]. In CVD techniques, the growth and properties of CNTs depend on the synthesis conditions, catalyst characteristics including composition, morphology, as well as the support used. Typically, nanotubes are grown using a method such as chemical vapor deposition (CVD) on metal catalyst particles or islands placed on top of a semiconductor or insulating substrate. However, for many envisioned applications, direct growth of nanotubes on a common conductive substrate such as copper would be beneficial to ensure good electrical contact. In this paper, topography and structural properties were investigated by atomic force microscopy (AFM) and scanning electron microscopy (SEM), respectively.

2. Experimental Details

Cu-Ni thin films with different thicknesses of Ni NPs layer were prepared on glass substrates by a capacitance-coupled RF-PECVD system with a 13.56 MHz power supply. The reactor consisted of two electrodes of different sizes. The smaller electrode was Cu and Ni targets as powered electrodes in the first and the second steps of deposition respectively and the other electrode was grounded substrates. The distance between the powered electrode and the substrate was maintained at 5 cm. The deposition was done at room temperature. The chamber was evacuated to a base pressure of about 10^{-5} mbar prior to the deposition and then the pressure was raised to the desired ambient pressure using acetylene gas flow. The deposition was done in two steps (Cu and Ni deposition). In the first step, for the growth of Cu NPs, the power was held at around 180 W, and the initial acetylene gas pressure was varied from 0.03 to 0.05 mbar. Ni of different thicknesses was grown over the Cu NPs. The deposition time for the Cu NPs was 20 min. After Cu deposition, Ni was sputtering during 2, 7, and 10 min with RF power of 230 W and initial acetylene gas pressure of 0.025 mbar. AFM (Veeco Instruments, Inc., USA) in the non-contact mode was used to obtain the surface morphology of the film and root mean square (RMS) roughness. The optical properties were performed using a double-beam UV-Vis spectrometer in the range of 300-800 nm.

3. Results and discussion

3.1 Structural properties of Cu-Ni thin films

The SEM images of CNTs grown on Cu NPs without Ni over layer and with 5, 10, and 15 nm of Ni over layers are shown in Figure 1(a-d). SEM is an experimental process that scans a sample with an electron beam to produce a magnified image for analysis. As shown in the SEM images, the size of CNTs increased from 5 to 15 nm in thickness for the deposited thin films, with a maximum value at 15 nm. A more significant feature is the thickness of the Ni layers, which affects the diameter of the CNTs. By adding the thickness of Ni, the density of the CNTs increases. It can be seen that in the SEM images, carbon nanotubes have different diameters, and in general, the average diameter of the grown nanotubes increases with the increase in the thickness of the nickel layers. Therefore, it can be concluded that nickel nanoparticles have a strong catalytic effect for making carbon nanotubes on copper nanoparticles in Cu-Ni thin films.

3.2 Surface morphological properties of Cu-Ni thin films

The surface morphology of the films was studied by using AFM. Figure 2(a-d) shows the 3D view of the surface AFM analysis of Cu-Ni thin films. All AFM images were obtained over square areas of 2 μm × 2 μm. With careful consideration of Figure 2(a, b), it is obvious that at the early step of Ni NPs layer deposition, Ni NPs grow on Cu NPs seeds for the film with 5 nm Ni during 2 min deposition, at the middle step of Ni NPs layer deposition, clusters of NPs are formed during 7 min deposition of Ni (10 nm Ni NPs layer) is shown in Figure 2(c). In Figure 2(d), aggregation of NPs becomes seen for a film with 10 min deposition of Ni (15 nm Ni NPs layer). RMS roughness of surface film is obtained at 1.25, 1.55, 1.45 and 1.4 nm for the Cu NPs without Ni NPs over layer, and with 5, 10 and 15 nm of Ni NPs over layer, respectively. RMS roughness value increases for Figure 2(a) with respect to Figure 2(b) which confirms growth of Ni NPs on the Cu NPs seeds for film with 5 nm Ni NPs over layer. The reduction of RMS roughness for Figure 2(c, d) suggests aggregation of Ni NPs for film with 10 and 15 nm Ni NPs over layer. It turned out that the roughness of the film surface decreases with the increasing thickness of Ni over the layer and the surface of the films becomes smooth and brighter spots appear in AFM images.

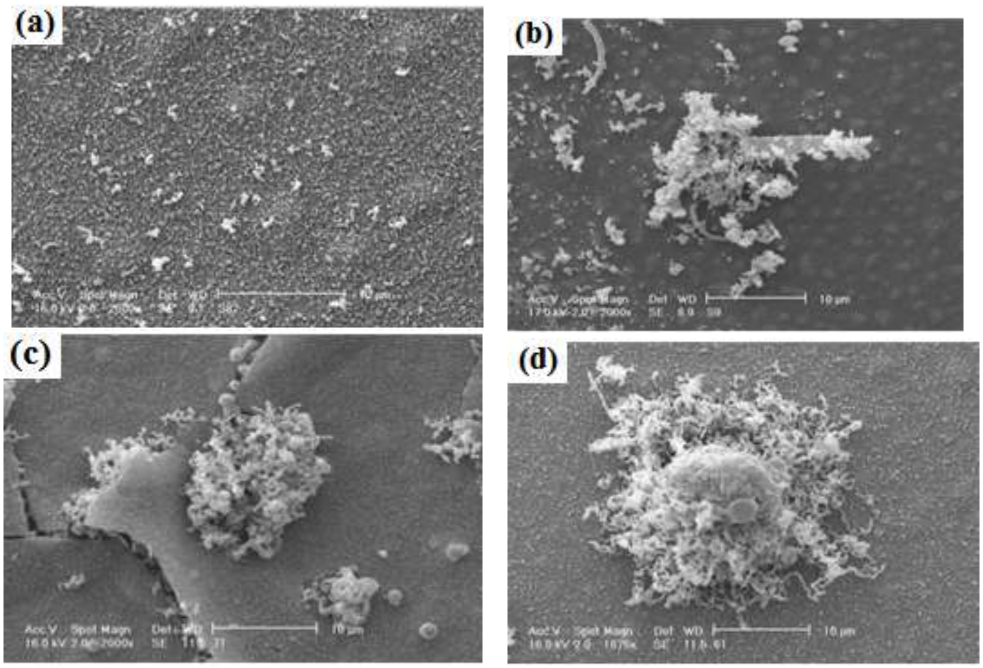

Fig.1 SEM images of Cu NPs **(a)** without Ni over layer and **(b)** with 5 nm, **(c)** 10 nm and **(d)** 15 nm of Ni over layer.

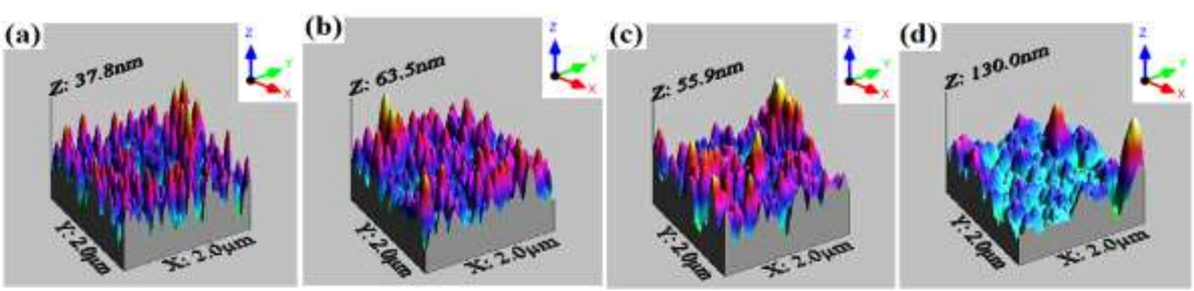

Fig.2 AFM images of Cu NPs **(a)** without Ni over layer and **(b)** with 5 nm, **(c)** 10 nm and **(d)** 15 nm of Ni over layer.

Figure 3(a-d) shows the variations in the height of the thin films on the surface versus the x and z axes for the Cu NPs without Ni NPs over layers, and with 5, 10 and 15 nm of Ni NPs over layer, respectively. The scanning size on the surface of the films was as much as 1 μm × 1 μm by the AFM, so the maximum numerical value on the x-axis was as much as 1 μm. The changes in height on the surface of the scanned films show that the films have a topological phase change with the variation of Ni thickness. Cu NPs without Ni have lower fluctuations, and the peaks have a slower slope than other thin layers contenting different thicknesses of Ni. Films with a thickness of 15 nm Ni compared to other films have a phase change of about 25 nm and indicate that the films, in this case, are firstly very smooth and secondly can have a phase change.

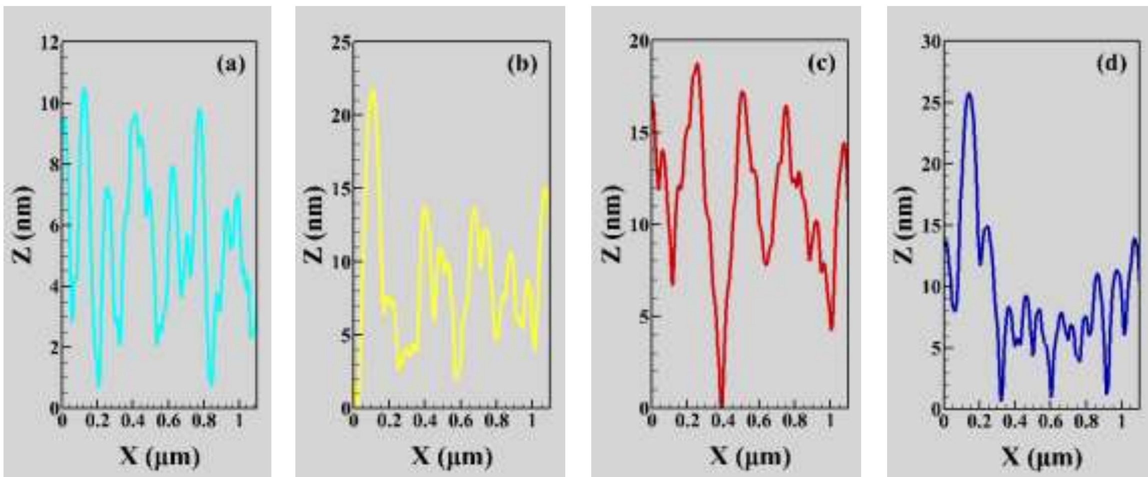

Fig.3 Z-height variations of nanoparticles on the surface versus x-axis of Cu NPs **(a)** without Ni over layer and **(b)** with 5 nm, **(c)** 10 nm and **(d)** 15 nm of Ni over layer.

Power spectral density (PSD) spectra were extracted from the scanned area and 1μ×1μ obtained from AFM images of the films as shown in Figure 4. It can be seen that all the PSD points contain a high spatial frequency region. According to dynamic scaling theory (DST), analysis of power spectral densities (PSDs) closely reveals how roughness changes with length scale. AFM images can be divided into pixels as a small square area, where h(xi) and h(yj) are the height vectors at the positions (xi, yj). Then, the one-dimensional average of the power spectral densities (PSDs) is presented as follows:

$$P(n) = \frac{2L}{N} \left[< \sum_{i=1}^{\frac{N}{2}} (FFT\ (h\ (x_i))^2 >_y + < \sum_{j=1}^{\frac{N}{2}} \left(FFT\ (h\ (y_j)\right)^2 >_x \right] \qquad (1)$$

That FFT is the Fast Fourier Transform between the real and reciprocal spaces. According to the dynamical scaling theory, for a system of lateral size L, the relation $P(k)$ and frequency k be written as [15]:

$$P(k) \propto k^{-\beta} \qquad (2)$$

That β is calculated as the slope of the log-log in PSD of high spatial frequency. Figure 4(a-d) shows the variations of spectral density with a spatial frequency of films for the Cu NPs without Ni NPs over layer and with 5, 10 and 15 nm of Ni NPs over layer, respectively. The spectral density power of all films reflects the reverse flow changes, especially in the high spatial frequency region, indicating the presence of fractal components in prominent topographies. These relative values determine surface irregularities at different distance scales. By the thicknesses of Ni layers were increased, the performance of the spectral compaction power increased.

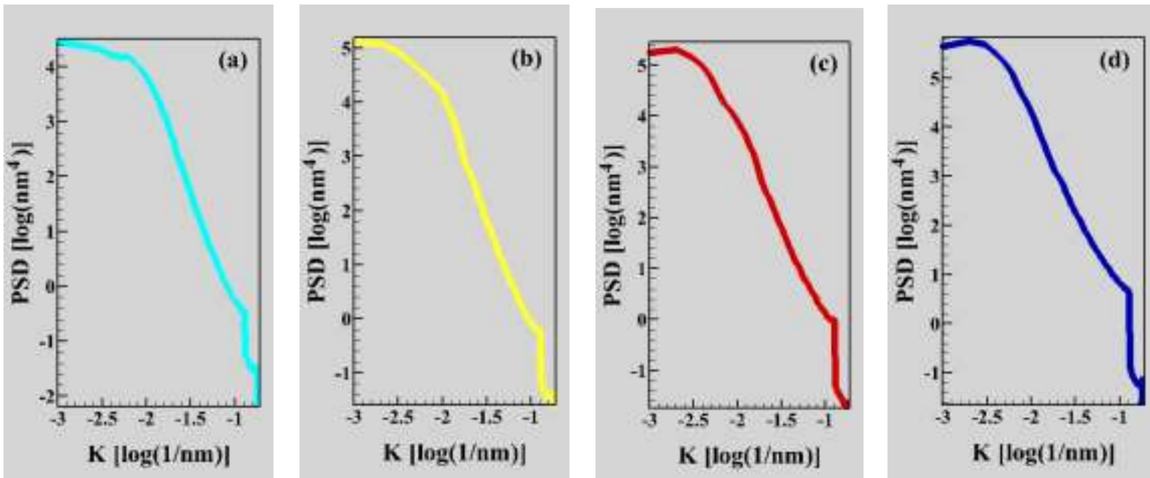

Fig.4 Power spectral density variations versus frequency k of Cu NPs **(a)** without Ni over layer and **(b)** with 5 nm, **(c)** 10 nm and **(d)** 15 nm of Ni over layer.

Figure 5(a-d) shows the variations of the bearing area versus the height of films for the Cu NPs without Ni NPs over layer and with 5, 10 and 15 nm of Ni NPs over layer, respectively. In fact, it indicates the amount of vacuum, zero coverage (cavity, bottom curvature of the diagram), monolayer (upper curvature of the diagram), and isolation (between the cavity and monolayer) of the thin films. Cu NPs without Ni, Cu NPs with 5 and 10 nm Ni have cavity coverage of less than 5% and layer content of about 90% and 95% which are monolayer height. In the vacuum, Cu NPs with 15 nm Ni, the coating is 10%, and the content of the film is about 90%, which is 80% isolated. Thickness did not have much effect on the degree of isolation, so all four diagrams have similar results.

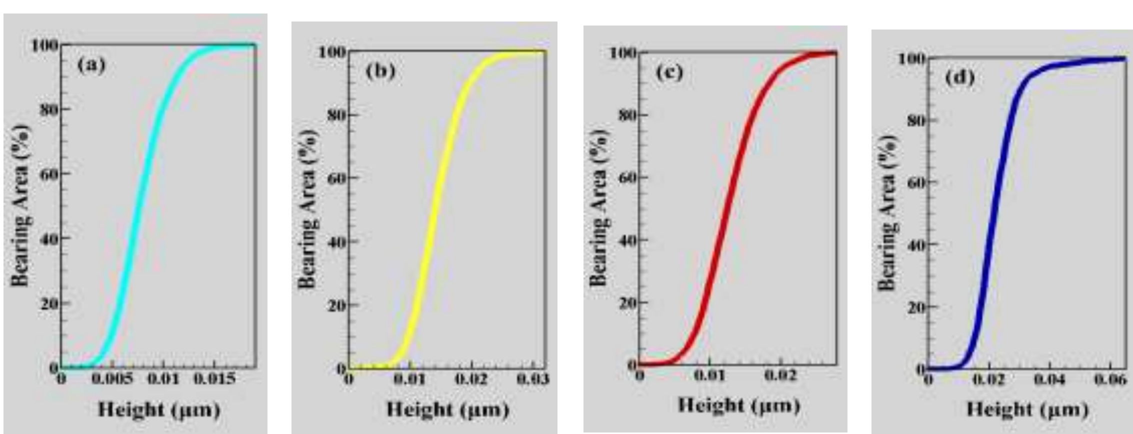

Fig.5 Bearing area variations of nanoparticles on films surface versus height of Cu NPs (a) without Ni over layer and (b) with 5 nm, (c) 10 nm and (d) 15 nm of Ni over layer.

3.3 Optical properties of Cu-Ni thin films

The absorption coefficient α of the thin film is obtained by the following equation [16]:

$$T = A \, Ln(-\alpha \, d) \rightarrow \alpha = 1/d^{*}Ln(1/T) \qquad (3)$$

The optical absorption coefficient of thin films versus incident photon wavelength is shown in Figure 5. The thickness of deposited films was 100 nm. The thickness d is measured using the DEKTAK 3 profilometer method. The change of optical absorption can be due to the change of local modes, free carriers and RMS roughness of the layers. The absorption coefficient of thin films with a thickness of 5 nm of Ni was higher than all thicknesses, and as a result, it had less light scattering. Therefore, the increase in the thickness of Ni influences the index of the absorption coefficient of Cu-Ni thin films.

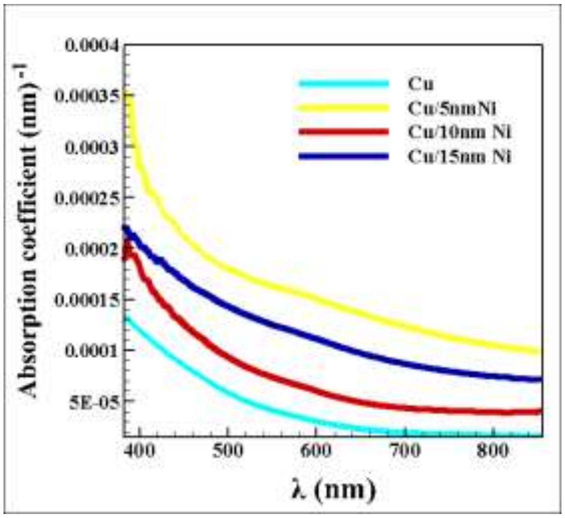

Fig.6 Variations of the absorption coefficient versus wavelength for Cu NPs without Ni over layer and Cu NPs with 5, 10 and 15 nm of Ni over layer.

4. Conclusions

According to SEM images, it can be seen that Carbon Nanotubes, CNTs, synthesized has the maximum value of the average diameter in the films deposited in the thickness of 15 nm of Ni. From AFM images, it turned out that the roughness of the film surface decreases with the increasing thickness of Ni over layer and the surface of films becomes smooth. The changes in height on the surface of the scanned films show that the films have a topological phase change. By the thicknesses of Ni layers were increased, the performance of the spectral compaction power increased. Thickness did not have much effect on the degree of isolation, so all four diagrams have similar results. The change of optical absorption can be due to the change of local modes, free carriers and RMS roughness of the layers.

References https://doi.org/10.1063/1.2947235.

[1] V. Dalouji, S. Elahi, S. Solaymani, A. Ghaderi, and H. Elahi, Carbon films embedded by nickel nanoparticles: fluctuation in hopping rate and variable-range hopping with respect to annealing temperature, Applied Physics A, 122(5), 2016, 541. https://doi.org/10.1007/s00339-016-0074-z.

[2] Y.Y. Chang, D.Y. Wang, and W. Wu, Catalysis effect of metal doping on wear properties of diamond-like carbon films deposited by a cathodic-arc activated deposition process, Thin Solid Films, 420, 2002, 241-247. https://doi.org/10.1016/S0040-6090(02)00801-5.

[3] S. Ţălu, M. Bramowicz, S. Kulesza, V. Dalouji, M. Ilkhani, A. Ghaderi, A. and S. Solaymani, Influence of annealing process on surface micromorphology of carbon–nickel composite thin films, Optical and Quantum Electronics, 49, 2017,1-9. https://doi.org/10.1007/s11082-017-1040-5.
[4] A. Arman, T. Ghodselahi, M. Molamohammadi, S. Solaymani, H. Zahrabi and A. Ahmadpourian, Microstructure and optical properties of Cu@ Ni nanoparticles embedded in aC: H, Protection of Metals and Physical Chemistry of Surfaces, 51, 2015 ,575-578. https://doi.org/10.1134/S2070205115040036.
[5] S. Singh, S. Basu and S.K. Ghosh, Structure and morphology of Cu/Ni film grown by electrodeposition method: A study of neutron reflectivity and AFM, Applied Surface Science, 255(11), 2009, 5910-5916. https://doi.org/10.1016/j.apsusc.2009.01.030.
[6] Y. Zhou, S. Wang, M. Xiao, D. Han, Y. Lu and Y. Meng, Formation of dimethyl carbonate on nature clay supported bimetallic copper-nickel catalysts, Journal of Cleaner Production, 103, 2015, 925-933. https://doi.org/10.1016/j.jclepro.2014.08.075.
[7] J. Bian, M. Xiao, S.J. Wang, Y.X. Lu and Y.Z. Meng, Graphite oxide as a novel host material of catalytically active Cu–Ni bimetallic nanoparticles, Catalysis Communications, 10(11), 2009, 1529-1533. https://doi.org/10.1016/j.catcom.2009.04.009.
[8] M. Zhang, K. Yang, X. Zhang and Y. Yu, Effect of Ni (111) surface alloying by Pt on partial oxidation of methane to syngas: A DFT study, Surface science, 630, 2014, 236-243.
[9] H. Dai, Carbon nanotubes: opportunities and challenges, Surface science, 500(1-3), 2002 , 218-241. https://doi.org/10.1016/j.susc.2014.08.023.
[10] S.A. Moshkalyov, A.L.D. Moreau, H.R. Guttiérrez, M.A. Cotta and J.W. Swart, Carbon nanotubes growth by chemical vapor deposition using thin film nickel catalyst, Materials Science and Engineering: B, 112(2-3), 2004, 147-153. https://doi.org/10.1016/j.mseb.2004.05.038.
[11] P.G. Collins, A. Zettl, H. Bando, A. Thess and R.E. Smalley, Nanotube nanodevice, Science, 278(5335), 1997, 100-102. https://doi.org/10.1126/science.278.5335.100.
[12] A.J. Song, M.Z. Ma, W.G. Zhang, H.T. Zong, S.X. Liang, Q.H. Hao, R.Z. Zhou, Q. Jing and R.P. Liu, Preparation and growth of Ni–Cu alloy nanoparticles prepared by arc plasma evaporation, Materials Letters, 64(10), 2010, 1229-1231. https://doi.org/10.1016/j.matlet.2010.02.061.
[13] C. He, N. Zhao, C. Shi, X. Du and J. Li, Synthesis of binary and triple carbon nanotubes over Ni/Cu/Al2O3 catalyst by chemical vapor deposition, Materials Letters, 61(27), 2007, 4940-4943. https://doi.org/10.1016/j.matlet.2007.03.077.
[14] V.I. Merkulov, A.V. Melechko, M.A. Guillorn, M.L. Simpson, D.H. Lowndes, J.H. Whealton and R.J. Raridon, Controlled alignment of carbon nanofibers in a large-scale synthesis process, Applied Physics Letters, 80(25), 2002, 4816-4818. https://doi.org/10.1063/1.1487920.
[15] V. Dalouji, S. Goudarzi and S. Solaymani, The optical density and topography characterizations of MWCNTs on Ni-Cu/a-C: H substrates with different copper percentage, Microscopy Research and Technique, 84(6), 2021, 1205-1211. https://doi.org/10.1002/jemt.23679.
[16] S. Goudarzi and V. Dalouji, The effect of Cu content in MWCNTs synthesized by Ni-Cu@ aC: H catalyst on the optical constants and the optical loss, Optik, 223, 2020, 165585. https://doi.org/10.1016/j.ijleo.2020.165585